1   **Combining colour parameters and geochemical tracers to improve sediment source discrimination**

2   **in a mining catchment (New Caledonia, South Pacific Islands)**

3   Virginie Sellier[1], Oldrich Navratil[2], John Patrick Laceby[3], Cédric Legout[4], Michel Allenbach[5], Irène

4   Lefèvre[1] , Olivier Evrard[1]

5   [1]Laboratoire des Sciences du Climat et de l'Environnement (LSCE), UMR 8212 (CEA/CNRS/UVSQ-IPSL),

6   Université Paris-Saclay, Gif-sur-Yvette (France)

7   [2] Laboratoire Environnement Ville Société (EVS), Université Lumière Lyon 2, UMR 5600 (CNRS), Lyon

8   (France)

9   [3] Alberta Environment and Parks, Calgary, Alberta (Canada)

10   [4]Institut des Géosciences de l'Environnement (IGE), UMR 5001, Grenoble (France)

11   [5]LIVE-EA 4243, Université de Nouvelle-Calédonie & LABEX Corail, Nouméa (Nouvelle-Calédonie,

12   France)

13   **Corresponding author:** selliervirg@free.fr ; Tel: (33)673910072

Abstract

15 Over the last century, human activities have induced significant land-cover changes that have

16 accelerated soil erosion processes around the world. In New Caledonia, a French island located in the

17 south-west Pacific Ocean, open-cast nickel mining has raised many concerns regarding its impact on

18 riverine systems (i.e. hyper-sedimentation, overburden) and the island's ecosystems (i.e. flooding,

19 lagoon siltation, water pollution).

20 A sediment tracing study has been conducted to quantify the contribution of mining versus

21 non-mining sub-catchments in one of the first areas exploited for nickel mining, the Thio River

22 catchment (397 km²). Sediment deposited during two cyclonic events (i.e. 2015 and 2017) was

23 collected following a tributary design approach. Source (n= 24) and river sediment (n= 19) samples

24 were analyzed by X-ray fluorescence and spectroscopy in the visible spectra (i.e. 365-735 nm). Four

25 fingerprinting approaches based on (1) colour parameters, (2) geochemical properties, (3) colour

26 parameters coupled with geochemical properties and (4) the entire visible spectrum were tested to

27 estimate sediment source contributions.

28 The results demonstrated that the individual sediment tracing methods based on spectroscopy

29 measurements (i.e. (1) and (4)) did not provide sufficient discrimination between sources. However,

30 the inclusion of colour properties in addition to geochemical parameters (3) provided the highest

31 discrimination between sources (i.e. 92.6 % of source variance explained). Although with a slightly

32 lower discrimination potential (i.e. 83.1 % of variance explained in sources), the geochemical

33 approach (2) provided similar results to those obtained with the colour coupled with geochemical

34 approach (3). In addition, mixed linear models associated with these two approaches have been

35 experimentally validated with artificial mixture samples. The results obtained with model (3) showed

36 that mining source contributions strongly dominated the sediments inputs with a mean contribution

37 of 68 % (SD 9 %) for the 2015 flood event and 88 % (SD 8%) for the 2017 flood event. These results

38 suggest that catchment management should focus on the contributions of mining tributaries to

39   reduce sediment inputs in the river systems. Therefore, the use of these approaches based on

40   geochemical properties individually (2) and coupled to colour parameters (3) could be extended to

41   other mining catchments of New Caledonia but also to other similar nickel mining catchments

42   around the world (e.g. Australia, Brazil, Dominican Republic, Cuba) to estimate sediment source

43   apportionment.

45   **Keywords:** Nickel mining • Sediment source fingerprinting • Soil erosion • Modeling

46

Introduction

47

48   At the dawn of a fourth industrial revolution, demand for metalliferous minerals continues to

49   increase and impact the world market (Prior et al., 2013;Highley et al., 2004). Currently, open-cast

50   mining generates more than three-quarters of the world's metal ores. However, the extraction of

51   these minerals is associated with deleterious impacts on the environment. In particular, these mines

52   are responsible for the increase in soil erosion and the transfer of sediment in river systems

53   worldwide (Yellishetty et al., 2013;Dumas et al., 2010;Abel et al., 2000).

54   New Caledonia, an island located in the south-western Pacific Ocean and currently the world's

55   sixth-largest producer of nickel, is in particular challenged with the problems of hyper-sedimentation

56   and over-burden of its river systems. Several studies outline how mining activities, which started in

57   1875, are generally responsible for these deleterious river morphological changes (Bird et al.,

58   1984;Iltis, 1992;Garcin et al., 2017). The excessive sediment inputs transferred mainly during

59   extreme rainfall events (e.g. cyclones and tropical depressions) lead to the increased occurrence of

60   flooding events in these tropical regions. Owing to the occurrence of major cyclones in New

61   Caledonia (i.e. on average one cyclone every 2.7 years (Garcin, 2010)), the local population regularly

62   have to deal with the damage generated by these flood events (e.g. damage to human settlements,

63   public infrastructure, agricultural land and, human casualties). Moreover, the island's agricultural and

64   fishing resources are also impacted.

65   Suspended sediment is known to transport large quantities of contaminants in river systems

66   (Vaithiyanathan et al., 1993;Bradley and Lewin, 1991). Hedouin et al. (2007), and more recently

67   Baudrimont et al. (2019), observed high concentrations of trace metals, including Ni and Cr, in

68   marine and freshwater organisms in New Caledonia. On a more global level, this anthropogenic

69   activity also threatens the second largest coral reef in the world, listed as a UNESCO World Heritage.

70   In particular, the increased turbidity associated with sediment supply could disrupt coral metabolism

71   (i.e. photosynthetic processes) (Juillot, 2019). These coral reefs provide an exceptional biological

72   diversity and deliver several essential ecosystem services to the local population including fisheries,

73   coastal protection and tourism (Pascal, 2010). The implementation of effective and perennial

74   sediment control measures on mining sites (e.g. sediment retention basin, revegetation) is therefore

75   required to reduce sediment inputs into the lagoon.

76   Erosion generated by open-cast nickel mining (i.e. mining bare soil, mining roads, mining

77   prospection and mining waste) do not provide the only sediment source in New Caledonia's mining

78   catchments. The use of fires to clear landscapes conducted by the local population for farming,

79   pasture and hunting increase the area of bare soils (Dumas et al., 2010). Soils that are left uncovered

80   by vegetation are more sensitive to erosion and they may be exposed to shallow landsliding (Blake et

81   al., 2009;Smith et al., 2011). Moreover, several invasive species such as deers or wild pigs also

82   threaten soil stability through trampling and overgrazing (Shellberg et al., 2010).

83   The contribution of mining tributaries (i.e. draining mining areas) and non-mining tributaries

84   (i.e. draining areas without mining activities) to sediment transiting catchments in New Caledonia

85   therefore needs to be discriminated. This discrimination has particularly become important since the

86   mining industries are subject to the "polluter pays" principle applied since 1975, i.e. the obligation to

87   fund remediation according to the extent of the damage generated by mining activity on the

88   environment. There is therefore a real social, environmental and financial challenge in discriminating

89   between sediment sources generated by mining activities and other potential sediment sources.

90   Sediment fingerprinting techniques have been developed since the 1970s to determine the

91   spatial origin of sediment sources and quantify their contributions (Collins et al., 1996;Walling et al.,

92   1979). These techniques are based on the analysis of multiple conservative properties both in the

93   sediments and their potential sources. Fallout radionuclides (Wallbrink, 2004;Evrard et al.,

94   2015;Wallbrink et al., 1998;Evrard et al., 2020), geochemical (Collins et al., 1997;Laceby and Olley,

95   2015) and mineral properties (Klages and Hsieh, 1975;Walden et al., 1997) are the most frequently

96   used tracers to quantify sediment source contributions. The use of fallout radionuclides and

97   geochemical properties as potential tracers was investigated to quantify the sources of suspended

98   sediment in the Thio River catchment (397 km²), one of the first catchments in New Caledonia to be

99   mined for nickel. Geochemical properties provided promising results (i.e. 83.1 % of variance

100 explained in sources) while the fallout radionuclides proved to be unsuitable (i.e. non-discriminatory)

101 (Sellier et al., 2019). However, other less expensive, faster and possibly more efficient techniques

102 than the more conventional methods previously tested could be envisaged. For example,

103 spectroscopy in the mid-infrared (MIR) (Poulenard et al., 2009), the visible near-infrared (VNIR) and

104 the shortwave-infrared (SWIR) (Brosinsky et al., 2014) regions of spectra have been used to quantify

105 the sediment source contributions. It is also non-destructive and requires low quantities of sample

106 material. Spectroscopy could therefore meet both the need for a simple and rapid sediment tracing

107 method in a context where flood events are frequent.

108 Moreover, New Caledonia has a specific geological feature which is at the origin of its mineral

109 wealth: one third of its surface area is covered with peridotite massifs. The weathering of these rocks

110 enriched in Fe and transition metals such as Mn, Cr and Co results in the formation of Ni- and Fe-

111 rich smectite, serpentine, goethite and hematite. The oxidized minerals (i.e. goethite and hematite)

112 provide a particularly reddish-orange colour to mining sources that distinguishes them from non-

113 mining sources, which tend to be grey in colour. The differences made visually between the two

114 sources further encourage the analysis of sources by spectroscopy and especially spectroscopy in the

115 visible region of the spectrum (i.e. 365-735 nm). In particular, the colorimetric parameters derived

116 from the visible spectrum have been shown to be effective in discriminating sediment sources. Their

117 discrimination power has been tested both individually (Evrard et al., 2019;Martínez-Carreras et al.,

118 2010;Uber et al., 2019) and in combination with other tracers (e.g. geochemical properties (Tiecher

119 et al., 2015)) according to the conventional fingerprinting approach (i.e. statistical analysis and use of

120 a mixing model). A more alternative approach based on the entire visible spectrum with the partial

121 least square regression (PLSR) models has also been developed to trace origin of sediment sources in

122 the literature (Legout et al., 2013;Tiecher et al., 2015).

123   As part of this study, four sediment fingerprinting methods based on (1) colour parameters, (2)

124   geochemical properties, (3) colour parameters coupled with geochemical properties and (4) PLSR

125   models based on the whole visible spectrum were tested in the Thio River catchment. Source (n=24)

126   and river sediment (n=19) samples were collected following a tributary design approach and

127   analyzed by X-ray fluorescence and spectroscopy in the visible spectra (i.e. 365-735 nm). The

128   performance of each method to estimate sediment source contributions was evaluated order to

129   select the best technique to be applied in the Thio River catchment and possibly in other mining

130   catchments of New Caledonia. On a wider scale, the tracers retained in this study could be

131   considered as potential sedimentary tracers to estimate sediment source apportionment in other

132   similar nickel mining catchments around the world (e.g. Australia, Brazil, Dominican Republic, Cuba).

133   Materials and methods

134   **1.1.Study area**

135   Located in the southwestern Pacific Ocean, New Caledonia (18 500 km²) is made up of several

136   islands, the largest of which is *La Grande Terre* (17 000 km²). The Thio River catchment (397 km²) is

137   located on the east coast of this island (Figure 1-a). It has a mountainous relief, with an average

138   altitude of 416 m above sea level (i.e. minimum: 0 m, maximum: 1392 m, Figure 1-a) and an average

139   slope of 45%. Two dominant lithologies are present in the catchment: volcano-sedimentary

140   formations mainly located on the western part of the catchment and peridotite massifs concentrated

141   in the eastern part of the catchment. Cherts (22 %), sandstone (9 %), a mix of basalt, dolerite and

142   gabbro (6 %), polymetamorphic rocks (6 %) mainly constitute volcano-sedimentary formations

143   whereas peridotite massifs are composed of laterites (18 %), peridotites (17 %), serpentines (10 %)

144   and hazburgites (1 %) (Garcin et al., 2017) (Figure 1-b). The Thio River catchment is covered on 96%

145   of its surface by permanent vegetation. According to the mining registry, active and abandoned

146   mining sites and exploration cover 21 % of the catchment area (Figure 1-c).

147   The Thio River catchment is subject to a tropical climate characterized by the alternation of a

148   hot wet season (November-April; mean temperature of 27 °C) and a cooler dry season (May-October;

149   mean temperature of 20 °C). The mean annual rainfall in the Thio River catchment is 1620 mm

150   despite strong seasonal fluctuations with the highest levels of precipitation recorded during the

151   cyclonic season between January and March (700 mm, 1981-2008; Alric (2009)). Although they only

152   occur on average once every 2.7 years, cyclones or tropical depressions may supply more than 20 %

153   of the annual rainfall in only one day according to local meteorological records (Météo France).

154

155   Twelve major tributaries flow into the main stem of the Thio River (28 km long) (Figure 1-b).

156   Ninety-two percent of the river channel length are characterized with slopes lower than 5 %.

157   According to Surell's classification (1841), the Thio River can be considered as torrential except in its

158   estuarine section. In addition, the extensive bare soil surface associated with past mining activities

159   (~10 sites), ongoing mining operations (e.g. 2 sites: Thio Plateau, Camps des Sapins) and the

160   occurrence of 6 km² of mining roads exacerbate runoff production as they contribute to increased

161   river network connectivity (Alric, 2009). This generates extensive erosion processes that are evident

162   across the entire Thio catchment with the widespread occurrence of rills, gullies, landslides and

163   channel bank erosion (Danloux and Laganier, 1991).

164

165
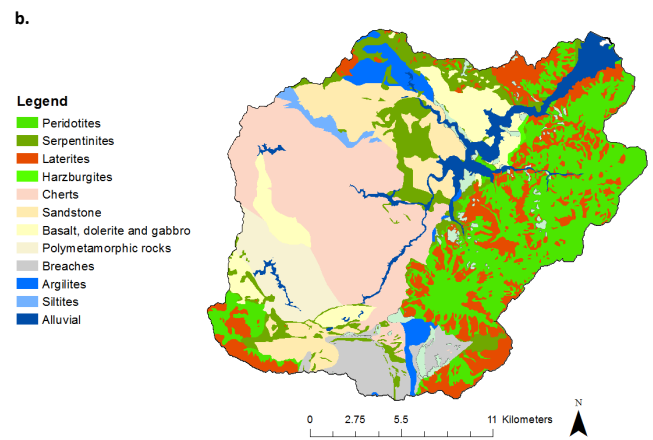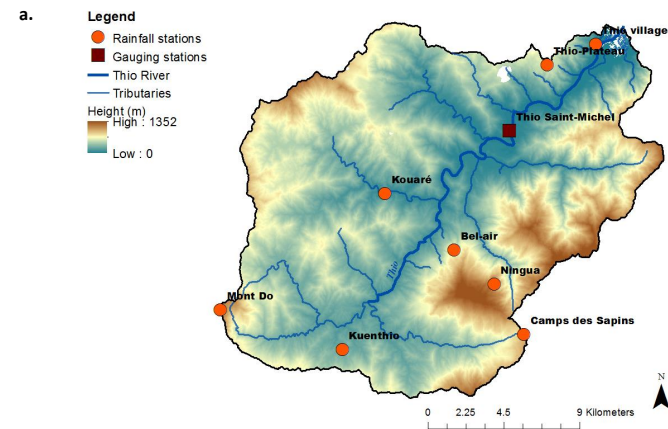
166
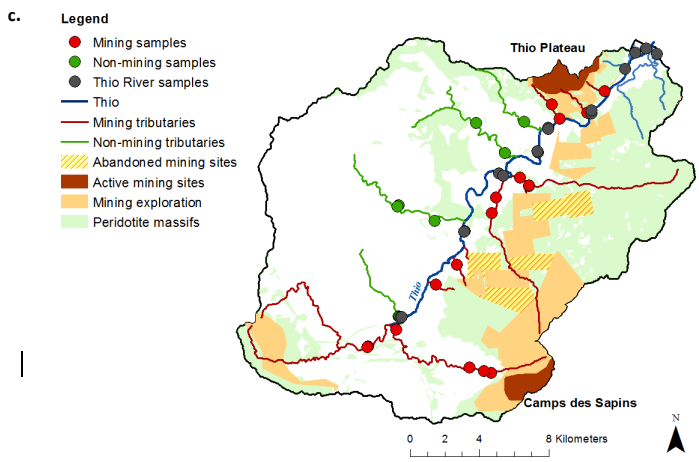
Figure 1 Location of the rainfall and river monitoring stations (a), main lithologies (b) and location of the sediment samples collected along with tributary source classifications (c) conducted in the Thio River catchment, New Caledonia

1.2. Hydro-sedimentary monitoring

169

170   Three rainfall stations (Thio Plateau, Thio village, Camps des Sapins; Figure 1-b) are operated

171   by Météo France and five others are managed by the DAVAR (Direction des Affaires Vétérinaires

172   Alimentaires et Rurales; i.e. Kouaré, Bel-Air, Ningua, Kuenthio, Mont Do), with daily records available

173   since 1952 for some stations (e.g. Thio village). Daily discharge has been monitored at a river gauging

174   station located on the main stem of the Thio River (at Saint-Michel) since 1981 by the DAVAR (Figure

175   1-a).

1.3. Sources and river sediment sampling

176

177   To trace the origin of sediment, lag deposits were collected as an alternative of suspended

178   sediment sampling on channel bars of mining tributaries (n= 16), non-mining tributaries (n= 8) and

179   the Thio River (n= 19) according to the tributary approach recommended by Laceby et al. (2017)

180   (Figure 1-c). They were sampled after two major floods (~10 year return period): (1) the tropical

181   depression of February 25, 2015 (n= 31) and (2) Cyclone Cook on April 10, 2017, (n= 12). These two

182   sample sets were respectively sampled between April 30 and May 5, 2015 and between May 16 and

183   17, 2017. At each sampling site, five to ten subsamples of fine sediment were collected across a 10

184   m² surface with a plastic trowel at exposed subaerial sites free of vegetation on channel bars. The

185   subsamples were composited into one sample representative of the fine sediment deposited on the

186   channel bars. The samples were oven-dried at 40°C for ~48 hours and sieved to 63 µm.

1.4. Preparation of artificial mixture samples

187

188   Equal quantities of all mining source samples (n= 16) were collected and mixed together to

189   create a composite sample of mining sources. The same process was carried out with non-mining

190   source samples (n= 8). The two composite samples respectively corresponding to mining and non-

191   mining sources were then mixed in known proportions to create artificial mixture samples (n= 21, 0-

192   100 % with a 5 % step, Table 1).

193 **Table 1** Proportions of mining and non-mining sources (%) in artificial mixture samples (M_i). *M6 was*

194 *withdrawn from this study because an error occurred at the time of its completion (out of study).*

M_i	Proportions of mining sources (%)	Proportions of non-mining sources (%)
M1	0	100
M2	5	95
M3	10	90
M4	15	85
M5	20	80
M6	*25 (out of study)*	*75 (out of study)*
M7	30	70
M8	35	65
M9	40	60
M10	45	55
M11	50	50
M12	55	45
M13	60	40
M14	65	35
M15	70	30
M16	75	25
M17	80	20
M18	85	15
M19	90	10
M20	95	5
M21	100	0

195

196 **1.5.Source, river sediment and artificial mixture sample analyses**

197 A portable diffuse reflectance spectrophotometer (Konica Minolta 2600d) was used to

198 measure the spectra in the visible (365-735 nm with a 10-nm resolution, 39-wavelength class) on

199 Thio River sediment (n= 19), tributary source (n= 16) and artificial mixture samples (n= 20). Sample

200 quantities between 0.1 g and 4 g were stored in 60 mL polystyrene tubes and analyzed at the Institut

201 des Géosciences de l'Environnement (IGE, Grenoble, France). Because of the rather small measuring

202 area (i.e. 3-mm radius circle), and to take into account the possible heterogeneity within the

203 samples, three measurements were carried out on river sediment and sources samples. For artificial

204 mixture samples, the experimenter who conducted the analyses carried out four measurements.

205 Several parameters (i.e. D65 illuminant, 10° angle observer and specular component excluded) were

206   applied for each measurement. Raw data collected corresponds to the spectral reflectance

207   percentage for each of the 39-wavelength class. From these raw data, 15 variables of various

208   colorimetry models were derived. Among these components, XYZ tri-stimulus values were calculated

209   based on the colour-matching functions defined by the International Commission on Illumination (CIE

210   1931). The standardized tri-stimuli were then converted into CIELab and CIELu'v' cartesian coordinate

211   systems using the equations provided by CIE (1976) and then into CIELch, CIEL*a*b* cartesian

212   coordinate systems using the equations provided by CIE (1994) (Rossel et al., 2006). First Derivative

213   reflectance of the Visible Spectra (FDVS) of each sample was also derived from the initial reflectance

214   spectrum. According to Tiecher et al. (2015), the use of FDVS avoids differences in baseline positions

215   and to get rid of the small differences due to uncontrolled sources of variation, as sample packaging.

216   Measurements of 11 geochemical elements (i.e. Mg, Al, Si , K, Ca, Ti, Cr, Mn, Fe, Ni and Zn) on

217   the samples were conducted by pre-calibrated energy dispersive X-ray fluorescence spectrometry

218   (Epsilon 3, Malvern PANalytical) with certified reference samples including Internal Atomic Energy

219   Agency (IAEA) standards (r^2 = 0.90-0.99, mean relative error: 9% ,SD 8 %, minimum: 1%, maximum:

220   23%). Between 0.2 and 0.5 g of the samples were packed in small mass holder (SMH) cells with an air

221   double X-ray Mylar film and analyzed at the Laboratoire des Sciences du Climat et de

222   l'Environnement (LSCE, Gif-sur-Yvette, France). Samples were irradiated with a primary beam

223   generated by an Rh anode X-ray tube emitting electromagnetic waves between 100eV and 1MeV

224   with a maximum power, typical current and voltage fixed to 15 W, 3mA and 50 kV respetively. The

225   associated Si-drift detector had a Be window thickness of 8 μm and recorded the sample spectrum in

226   a 2D optical geometry configuration. X-ray intensities were converted into concentrations using the

227   Epsilon 3 software program through the application of the fundamental parameters method.

228   **1.6.Statistical analysis and sediment tracing**

229   1.6.1.Conventional mixing model

230   In general, the sediment source fingerprinting approach is composed of four main steps: (1)

231   range test, (2) the Mann-Whitney U test, (3) a stepwise discriminant function analysis and (4) a

232   mixing model (Collins et al., 199 or the range test, all variables exhibiting values in the river

233   sediment samples that were outside of the range found in the potential sources (i.e. between the

234   minimum and maximum values found in source samples) were excluded from the analysis. It is

235   important to restrict the tracing parameters to those that show a conservative behavior to avoid

236   incorrect source prediction and consequently inaccurate estimations of source contributions (Sherriff

237   et al., 2015). Thereafter, the Mann-Whitney U test (α= 0.05, p-value <0.01) was performed to

238   evaluate whether remaining variables could discriminate the source samples. A stepwise

239   discriminant function analysis (DFA) was independently run on three set of potential tracing

240   properties: (1) colour parameters (i.e. 'colour'), (2) geochemical properties (i.e. 'geochemistry') and

241   (3) colour parameters and geochemical properties (i.e. 'colour + geochemistry'). For the last set, the

242   raw values of the variables were normalized in order to make them comparable. Indeed, several

243   colour parameters were within an order of magnitude of around 0.01 whereas for the geochemical

244   parameters the difference was around 10^6 mg kg^{-1} which resulted in a poorly conditioned matrix for

245   the DFA.

246   The following calculation was therefore applied on the variable values to normalize them: x_i –

247   x_{min}/ x_{max} - x_{min} where xi was value found in source sample (i), x_{min} and x_{max} were respectively the

248   minimum and maximum values found in the source samples. The DFA was carried out to select the

249   optimal number of potential tracers to discriminate the sources for each modelling approach with

250   the optimal number of potential tracers which must provide the lowest Wilks' lambda value from

251   analysis of variance. Indeed, the closer the Wilks' lambda value is to 1, the lower the variability within

252   the sources compared to the total variability. The DFA was performed in the backward mode with a p

253   >0.01 used to select a tracer and p <0.01 used to remove a tracer.

254   Finally, a classical solver-based mixing model was used to model the source contributions from

255   the mining and non-mining tributaries to target sediment through simultaneously minimizing the

256   mixing model difference (MMD) (Evrard et al., 2019):

257     $$MMD = \sum_{i=1}^{n} ((C_i - (A_i x + B_i(1-x))/C_i) \quad Equation\ 1$$

258   where n is the number of parameters in the model chosen by the selection process (i.e. steps 1, 2, 3);

259   C_i is the Thio River sediment sample parameter (i); x and (1-x) were respectively the contributions of

260   source A and B (i.e. mining and non-mining tributaries); A_i is the mean of parameter (i) in source A

261   and B_i is the mean of parameter (i) in source B. The proportional contribution from each source (x)

262   was modelled by solving Equation 1 with the Solver Function in Microsoft Excel with x being between

263   0 and 1 and the sum of source contributions (i.e. x and 1-x) equaling 1. The GRG Non-Linear solving

264   method was used with automatic scaling in Solver, ignoring integer constraints, with a maximum run

265   time of 5000 and allowing for 2500 iterations. A multi-start population size of 2500 was used along

266   with the same random seed for each of the model runs while requiring bounds on the variables. A

267   constraint precision and convergence of $1.0\ 10^{-6}$ were selected. To test the reliability of the 'colour',

268   'geochemistry' and 'colour + geochemistry' models, these latter were tested on artificial mixture

269   samples.

270   1.6.2.FDVS- PLSR model

271   FDVS-PLSR models were built following the methodology described in Poulenard et al. (2012).

272   The first step consisted in applying a principal component analysis (PCA) to evaluate the overall

273   variability between FDVS (i.e. 38 wavelengths) of source samples. Subsequently, a discriminant

274   analysis (DA) was conducted based on the PCA scores. The purpose of this analysis was to compare

275   the Mahalanobis distance between sources samples and to determine if FDVS of source samples

276 could discriminate the sources. Relationships between FDVS (x variate) and the corresponding weight

277 contribution of the sediment source data sets (y variate) were analyzed using PLSR. The PLSR models

278 were carried out based on the component set providing the lowest predictive error (PRESS, option on

279 XLStat software). Two independent PLSR models were built to estimate the two sediment source

280 contributions. As the artificial mixtures were measured four times by spectroscopy, 84 FDVS of

281 artificial mixture samples were generated including 50 values that were randomly selected to build

282 the models (training set (ST)) and 34 to validate the models (validation set (SV)). The SV:ST ratio used

283 was approximately 1:2, which is in agreement with recommendations provided in the literature

284 (Daszykowski et al., 2002). To evaluate the performance of PLSR models, several indicators such as

285 coefficient of linear regression (r^2), root mean square error of calibration (RMSEC) and root mean

286 square error of prediction (RMSEP) values were calculated. Unlike the conventional fingerprinting

287 approach, the estimated contributions of sources were not limited to be in the range of 0 % and 100

288 %. In a similar way, the sum of source contributions was not constrained to be equal to 100 %. As a

289 result, another way to control the reliability of predictions was to sum the prediction proportions of

290 both models (Legout et al., 2013). FDVS of river sediment samples were then introduced into these

291 PLSR models to estimate the contribution of sediment sources.

292 Results

293 **1.7. Source description**

294   The ranges of values of all colour parameters measured in the Thio River sediment samples

295 systematically plotted within the range of values observed in the two potential sources (i.e. mining

296 and non-mining tributaries; Figure 2 and Table 2). The range test results confirmed the conservative

297 character of these parameters. For geochemical properties, elemental concentrations measured in

298 the river sediment also plotted within the range of concentrations found in sources (Sellier et al.,

299 2019). According to the range test results, all properties were determined to be conservative.
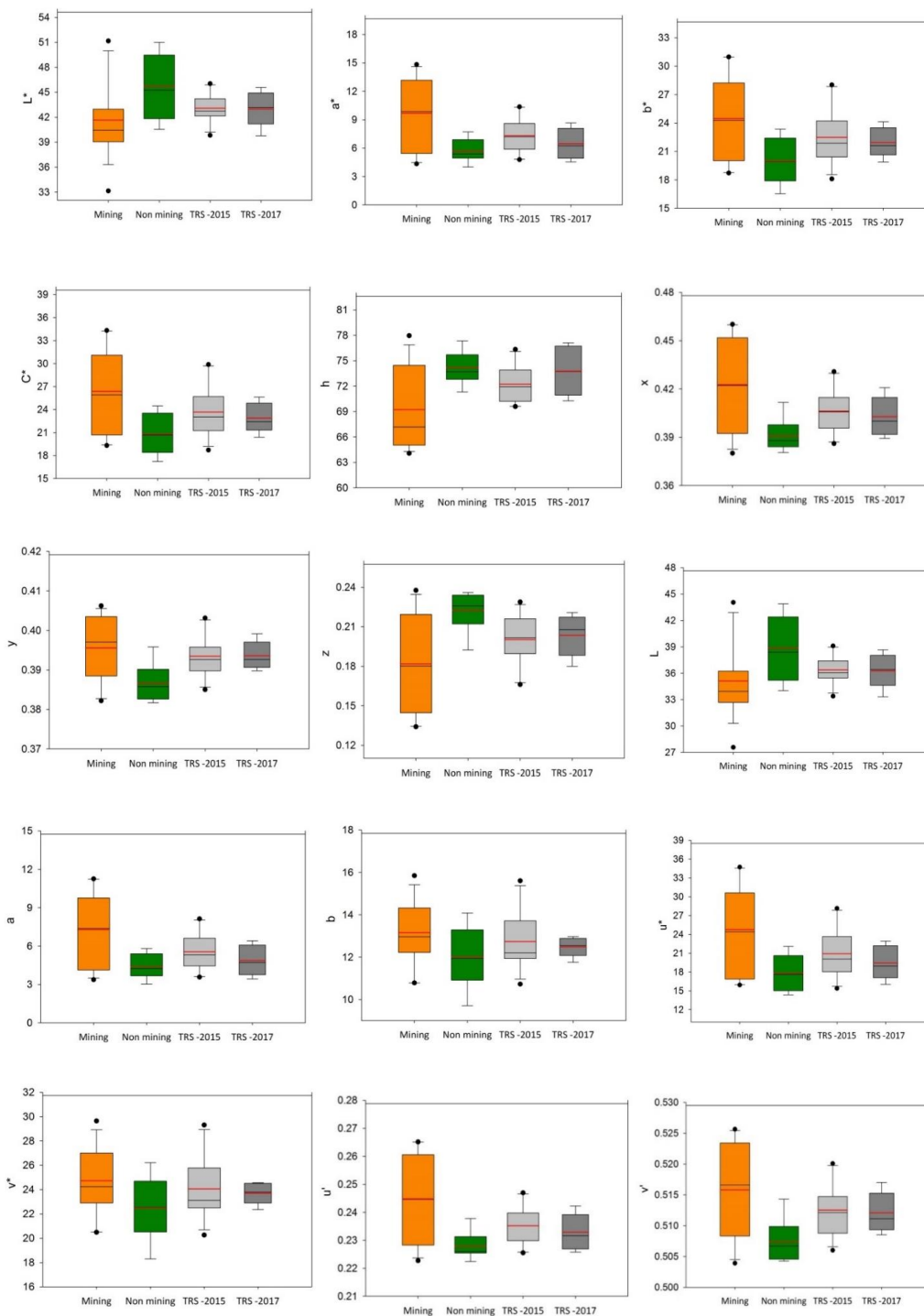
Figure 2 Box-plots of colour parameter values in the <63 μm fraction of sediment collected on the mining

tributaries (Mining), non-mining tributaries (Non-mining) and the main Thio River (Thio River sediment (TRS)-

flood events of 2015 and 2017). The box indicates the location of the first and third quartiles; the black line

indicates the median value; the red line indicates the mean value

304 **Table 2** Geochemical element content and colour parameter values in the <63 µm fraction of sediment sources

305 and Thio River sediment; results of Mann-Whitney U test and individual DA used to identify the potential

306 tracers to differentiate sources supplying sediment to the Thio River

Fingerprinting property	Mann-Whitney U test		DA- correctly classified samples (%)	Mining tributaries (n= 16)	Non-mining tributaries (n= 8)	Thio River sediment 2015 (n= 11)	Thio River sediment 2017 (n= 8)
	U-value	p-value					
Geochemical tracers							
Al *(g kg⁻¹)*	8	0.000	87.5	21 ± 21	67 ± 8	43 ± 15	29 ± 6
Ca *(mg kg⁻¹)*	21	0.007	62.5	3731 ± 470	9286 ± 5194	5281 ± 1201	3945 ± 666
Cr *(mg kg⁻¹)*	124	< 0.0001	83.3	7480 ± 4606	706 ± 967	4359 ± 2185	5715 ± 1786
Fe *(g kg⁻¹)*	121	0.000	91.6	144 ± 70	62 ± 24	43 ± 15	29 ± 6
K *(mg kg⁻¹)*	2	< 0.0001	95.8	1657 ± 2160	14019 ± 3702	5944 ± 3294	3750 ± 974
Mg *(g kg⁻¹)*	119	0.000	83.3	99 ± 59	16 ±13	88 ± 33	117 ± 21
Mn *(mg kg⁻¹)*	108	0.006	83.3	2531 ± 1317	1439 ± 606	2068 ± 667	1786 ± 516
Ni *(mg kg⁻¹)*	125	< 0.0001	91.6	6576 ± 5075	358 ± 339	4218 ± 1938	4341 ± 1239
Si *(g kg⁻¹)*	6	< 0.0001	91.6	178 ± 42	254 ± 28	221 ± 15	204 ± 7
Ti *(mg kg⁻¹)*	13	0.001	87.5	1409 ± 2077	5446 ± 835	2771 ± 1197	1663 ± 457
Zn *(mg kg⁻¹)*	68	0.834	-	146 ± 47	125 ± 4	134 ± 17	125 ± 8
Colour parameters							
L*	24	0.013	-	41.6 ± 4.6	45.7 ± 3.9	43.1 ± 1.7	43.0 ± 2.0
a*	104	0.013	-	9.7 ± 3.8	5.7 ± 1.2	7.3 ± 1.9	6.5 ± 1.7
b*	106	0.009	70.8	24.5 ± 4.5	20.0 ± 2.5	22.5 ± 3.0	21.9 ± 1.6
C*	108	0.006	66.6	26.4 ± 5.5	20.8 ± 2.7	23.7 ± 3.5	22.9 ± 2.0
h	26	0.019	-	69.2 ± 4.8	74.2 ± 1.9	72.2 ± 2.2	73.8 ± 2.9
x	107	0.007	75	0.42 ± 0.03	0.39 ± 0.01	0.41 ± 0.01	0.40 ± 0.01
y	111	0.003	79.2	0.396 ± 0.008	0.387 ± 0.005	0.393 ± 0.005	0.394 ± 0.004
z	19	0.005	75	0.18 ± 0.04	0.22 ± 0.01	0.20 ± 0.02	0.20 ± 0.02
L	27	0.013	-	35.1 ± 4.2	38.9 ± 3.7	36.4 ± 1.6	36.3 ± 1.9
a	103	0.016	-	7.3 ± 2.9	4.4 ± 1.0	5.6 ± 1.5	4.9 ± 1.2
b	91	0.106	-	13.1 ± 1.5	12.0 ± 1.5	12.7 ± 1.4	12.5 ± 0.4
u*	101	0.023	-	24.8 ± 6.9	17.8 ± 2.8	20.9 ± 4.0	19.4 ± 2.7
v*	93	0.081	-	24.7 ± 2.8	22.5 ± 2.7	24.1 ± 2.6	23.7 ± 0.8
u′	105	0.011	-	0.245 ± 0.016	0.228± 0.005	0.235 ± 0.007	0.233 ± 0.007
v′	111	0.003	79.2	0.516 ± 0.008	0.507 ± 0.004	0.513 ± 0.004	0.512 ± 0.003

307

1.8. Selection of parameters/properties for modelling

1.8.1. 'Colour' model

According to the Mann-Whitney U test results, six colour parameters (*i.e.* b*, C*, x, y, z, v')
provided significant discrimination between the two sediment sources (*i.e.* p-value < 0.01, Table 2).
The backward DFA selected only v' as the optimal tracer of mining and non-mining source sediments
(Figure 2, Table 3). Although this parameter correctly classified 79.2 % of sources, the high Wilk's
lambda value obtained (i.e. 0.7209, Table 3) induced that only 27.9 % of variance was explained by v'.
The low Mahalanobis distance value obtained (i.e. 1.6) confirmed that sediment sources were not
well separated. Accordingly, and owing to the high error percentage of the source discrimination
provided by this approach (i.e. 72.1 %), source contributions were not modeled with the 'colour'
model.

1.8.2. 'Geochemistry' model

When considering the two potential sediment sources, all geochemical properties (except Zn)
were selected as potentially discriminant by the Mann-Whitney U test (i.e. p-value < 0.01, Table 2).
Among the 10 potential tracers, K was selected by the backward DFA to model sediment source
contributions from mining and non-mining tributaries with 95.3 % of sources correctly classified and
83.1 % of variance explained by K. This percentage of variance explained was deduced from the final
Wilk's lambda value obtained (i.e. 0.1691). Moreover, the Mahalanobis distance value showed that
the sediment sources were well separated from each other with a significant distance of 20.3 (Table
3) (Sellier et al., 2019).

1.8.3. 'Colour + geochemistry' model

When combining colour parameters and geochemical properties, the DFA selected five optimal
tracers (i.e. K, Ca, Ti, b*, C*) able to correctly classify 100 % of the sources. A significant improvement
in the source discrimination was observed with the lowest Wilk's lambda value obtained (i.e. 0.0734)
and the highest percentage of variance explained (i.e. 92.6 %). Moreover, the Mahalanobis distance

333   value obtained (i.e. 52.1) was more than 2.5 times higher than that estimated with the

334   'geochemistry' model (Table 3), thus resulting in a better separation between sediment sources than

335   the previous approach (i.e. 'geochemistry')

336   **Table 3** Results of DFA used to identify the optimum tracer combination to differentiate sources supplying

337   sediment to the Thio River

Fingerprint property selected	Wilks'Lambda	Variance explained by the variables (%)	Squared Mahalanobis distance	Correctly classified samples (%)
'Colour'				
v'	0.7209	27.9	1.6	79.2
'Geochemistry'				
K	0.1691	83.1	20.3	95.3
'Colour + Geochemistry'				
K, Ca, Ti, b*, C*	0.0734	92.6	52.1	100

338

1.9. Assessment of model performance on artificial mixture samples

340   Prior to applying mixing models to river sediments, preliminary tests were conducted to

341   control the validity of the models (i.e. 'geochemistry' and 'colour + geochemistry') and the associated

342   estimations of source contribution errors. When applying these models on the artificial mixture

343   samples, actual and predicted proportions were well correlated for both models (i.e. r^2= 0.99 and r^2=

344   0.98 respectively for 'geochemistry' and 'colour + geochemistry' models) (Figure 3).

345   However, the 'geochemistry' model described in Figure 3-a showed that the contributions of

346   mining tributaries were overestimated. With 100 % of actual mining contributions, 100 % of mining

347   contribution was predicted by the model. However, instead of 0 % of actual mining contributions, a

348   mining contribution of 15.5% was predicted by the model. It means that the more the estimated

349   mining source contributions tends towards 0%, the greater the associated overestimation (i.e.

350   maximum 15.5 %) (Figure 3-a). The 'colour + geochemistry' model also provided a slight

351   overestimation of the contribution of mining tributaries (i.e. 7 % intercept of the regression line,

352   Figure 3-b). Given the slope of the regression line calculated is close to 1 (i.e. 0.98), this 7%

353   overestimation remains constant over the entire range of potential contributions.

354   **Figure 3** Comparison between actual mining source proportions prepared in artificial mixtures and the mining
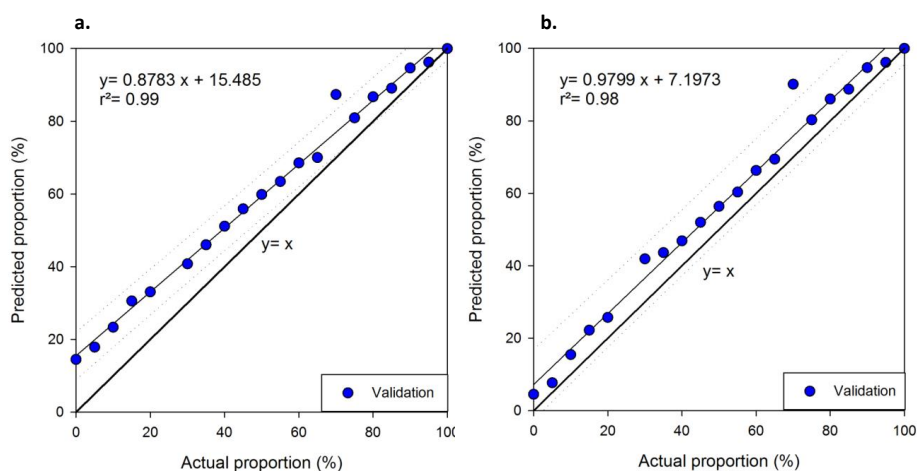
355   source proportions predicted by the 'geochemistry' (a) and 'colour + geochemistry' (b) models

356   **1.10. Building partial least-squares models based on FDVS**

357   Mining sources are characterized by a red-orange color while sediments originating from non-

358   mining sources are grey. The color contrasts may be explained by the distinct geochemical

359   composition of these sources. Mean FDVS indicated the presence of goethite (i.e. at 445 and 525

360   nm), hematite (i.e. at 555, 565 and 575 nm), and organic matter (i.e. between 600-700 nm) (Debret

361   et al., 2011) in both mining and non-mining sources (Figure 4). In similar way, the Thio River sediment

362   samples (2015, 2017) showed similar characteristics since the variations of the mean FDVS remained

363   between those found in the sources (Figure 4). Nevertheless, some differences can be observed

364   between the sources. The spectral signature of goethite is slightly stronger at 445 nm in non-mining

365   tributaries compared to mining tributaries. No difference between sources was observed at 525 nm,

366   the second wavelengths characterizing the presence of goethite. In contrast, the spectral signature of

367 hematite (*i.e.* at 555, 565 and 575 nm) was stronger in mining tributaries than in non-mining

368 tributaries.
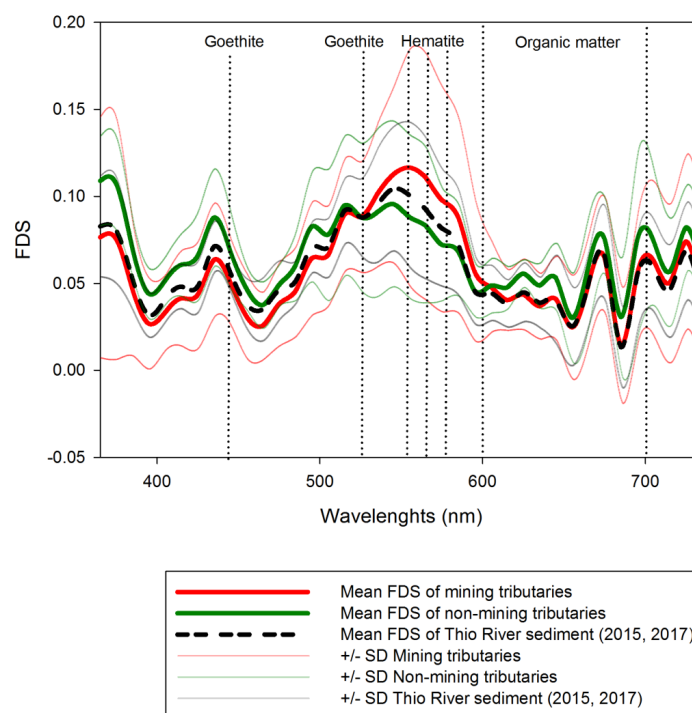
369 **Figure 4** FDVS measured in the <63 µm fraction of sources and Thio River sediment samples

370   To test the potential discrimination offered by FDVS, a PCA was applied on the source data set.

371 The first ten principal components from PCA explained 99 % of the total variation in the spectra. The

372 DFA performed on these components resulted in a final Wilks' lambda value of 0.1585. It means that

373 84.1 % of variance is explained by these ten components. Moreover, 100 % of the source samples

374 were correctly classified. The performances of FDVS-PLSR models are presented in Figure 5. The

375 mining and non-mining tributary FDVS-PLSR models provided an excellent correlation between actual

376 and predicted proportions with r^2 and slopes close to 1 and intercepts of linear regression close to 0.

377 The root mean square error of calibration (RMSEC) values estimated for both models were low, i.e.

378 3.4 % and 3.1 % respectively for mining and non-mining tributary models. These models also

379   provided a good predictability of source contributions with low root mean square error of prediction

380   (RMSEP) values (i.e. 8.0 % and 4.7 % respectively for mining and non-mining tributary models).

381   Another way to control the reliability of predictions was to sum the predicted proportions of both

382   models (Legout et al., 2013). Considering the whole data set used in the construction of the partial

383   least-squares regression models (i.e. calibration and validation) led to a mean sum of the predicted

384   source proportions of 102 % (SD 3 %, range: 98-114 %), thus highlighting the effective prediction

385   performance of FDVS-PLSR models.
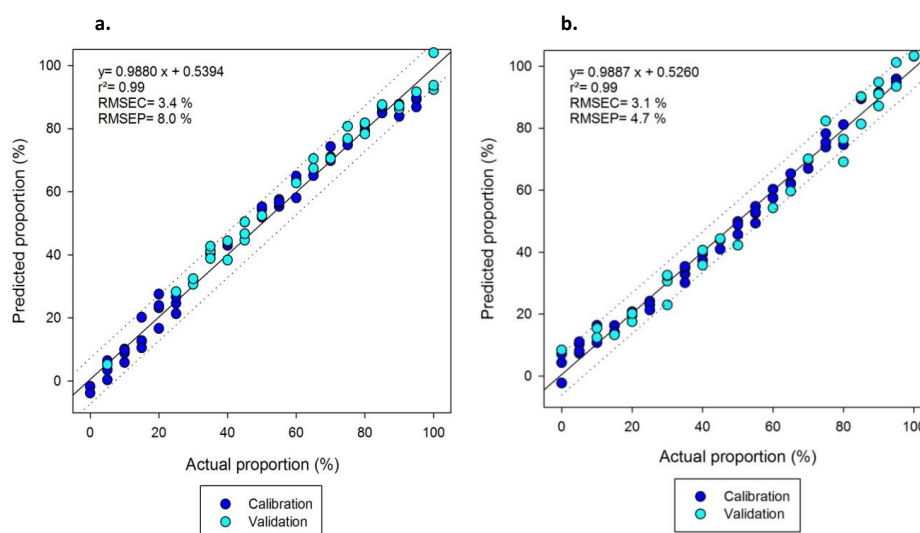
386   **Figure 5** Building of FDSV-PLSR models for mining sources (a) and non-mining sources (b)

387   **1.11.Source apportionment modelling**

388   1.11.1.'Geochemistry' model

389   The 'geochemistry' model estimated that the mining tributaries contributed an average of 65

390   % (SD 27 %) of the Thio River sediment during the 2015 flood event; they therefore dominated

391   sediment inputs overall during this event. Nevertheless, non-mining tributaries locally and mainly

392   contributed to the sediment inputs at three sampling points along the Thio River (Figure 6-a, Table 4,

393   sampling points [3, 5, 7]). These contributions did not, however, compensate those provided by

394   mining tributaries in the estuary (63-89 %). Indeed, the dominant mining contributions found in

395   upstream river reaches (96 %, Figure 6-a, Table 4, sampling point [1]) gradually decreased along the

396   Thio River, fluctuating between 17-77 % before increasing again at the confluence between the Thio

397   River and the mining tributaries draining the Thio Plateau mining area (i.e. 85 %, Figure 6-a, Table 4,

398   sampling point [8]) and reaching 60-64 %.

399

400   This model also demonstrated that mining tributaries dominated sediment inputs with a mean

401   contribution of 83 % (SD 8%) during the 2017 flood event (Table 5). The lowest mining tributary

402   contributions estimated (i.e. 69 %) was found after the confluence with the Kouaré non-mining

403   tributary (Figure 6-b, Table 5, sampling point [4]). Nevertheless, further downstream, the proportions

404   of the mining sources increased again to reach 77-83 % in the estuary (Figure 6-b, Table 5, sampling

405   points [7, 8]).

406
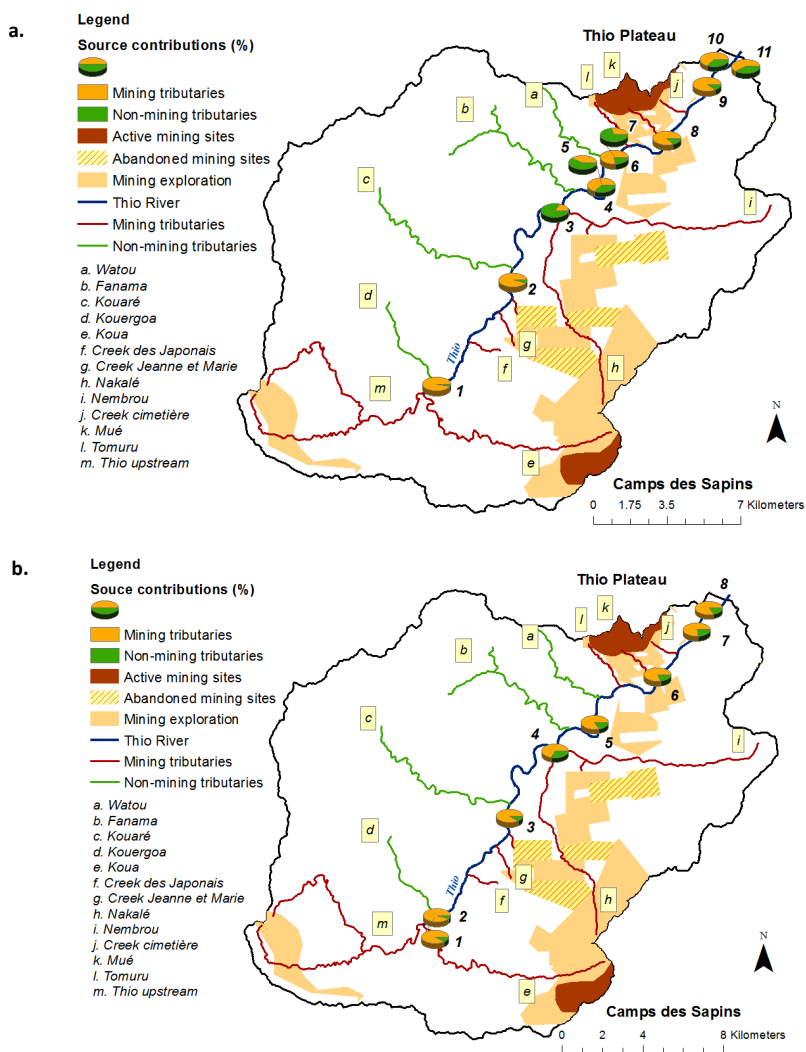
Figure 6 Relative contributions of mining and non-mining tributaries to the sediment collected in the Thio River during the 2015 (a) and 2017 (b) flood events using the 'geochemistry' model

410   1.11.2. 'Colour + geochemistry' model

411   Similar results were obtained with the 'colour + geochemisty' model. The contributions of

412   mining tributaries were estimated to an average of 68 % (SD 25 %) for the 2015 flood event. Mining

413   tributary contributions provided almost all the sediment transiting the uppermost reach of the Thio

414   River (i.e. 99 %, Figure 7-a, Table 4, sampling point [1]). However, after the confluence with the

415   Kouaré tributary, non-mining tributaries dominated with a contribution of 83 % (Figure 7-a, Table 4,

416   sampling point [3]). Further downstream, the contribution of mining tributaries increased again with

417   supplies varying between 34- 89 % to reach 58- 70 % in the estuary (Figure 7-a, Table 4). The largest

418   difference between 'geochemistry' and 'colour + geochemistry' model outputs was 18 % for the 2015

419   flood event.

420   The 'colour + geochemistry' model also demonstrated that 88 % (SD 8 %) of the sediment

421   supply originated from mining tributaries during the 2017 flood event. Along the Thio River, mining

422   tributary contributions varied between 100 % in the uppermost reach, 74% after the Kouaré river

423   confluence and 83-85% in the estuary (Figure 7-b, Table 5). The largest difference between

424   'geochemistry' and 'colour + geochemistry' model outputs was 10 % for the 2017 flood event (Table

425   5).

426
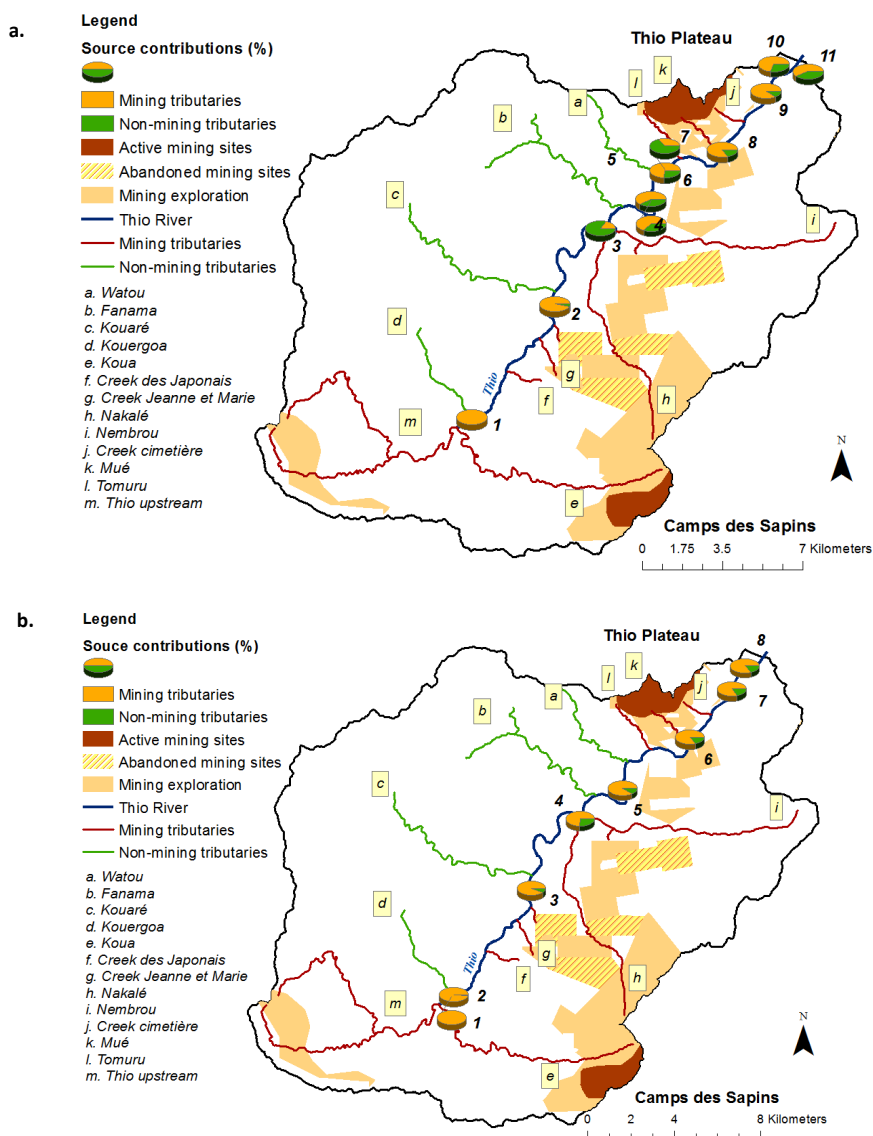
Figure 7 Relative contributions of mining and non-mining tributaries to the sediment collected in the Thio River
during the 2015 (a) and 2017 (b) flood events using the 'colour + geochemistry' model

429   1.11.3.FDVS-PLSR model

430   When applying the FDVS-PLSR models (i.e. mining and non-mining tributary contributions) to

431   the river sediment samples (2015, 2017), the mean sums of the source contributions were 92 % (SD 8

432   %) and 80 % (SD 13 %), respectively, for the 2015 and 2017 flood events (Tables 4 and 5). Owing that

433   predicted sums were different from the expected 100%, a bar plot display of the source contributions

434   has been chosen to facilitate the interpretation of the results (Figure 8).

435   According to the FDVS-PLSR model results, 34 % (SD 22 %) of sediment supply originated from

436   mining tributaries while non-mining tributary contribution provided 58 % (SD 18 %) of the sediment

437   input for the 2015 flood event (Figure 8-a, Table 4). In the upper part of the Thio River catchment,

438   non-mining tributaries largely dominated with a contribution of 80 % versus 6 % for mining

439   tributaries. Along the Thio River, mining tributary contributions gradually increased to reach 70 %

440   after the Mué tributary confluence (i.e. one of tributaries draining the Thio Plateau Mine, Figure 8-a,

441   Table 4, sampling point [9]). The non-mining tributary contributions fluctuated along the Thio River

442   between 41-85 % (Figure 8-a, Table 4, sampling points [2-8]) and reached a minimum (i.e. 28 %,

443   Figure 8-a, Table 4, sampling point [9]) after the Mué tributary confluence. In the estuary, sediment

444   supply was originated from 51-70 % of mining tributaries and 28- 52 % of non-mining tributaries

445   (Figure 8-a, Table 4, sampling points [9, 10, 11]).

446   The FDVS-PLSR models also indicated that mining and non-mining tributaries respectively

447   contributed a mean of 29 % (SD 20 %) and 51 % (SD 11 %) of sediment (Figure 8-b, Table 5) during

448   the 2017 flood event. In a similar way, mining contributions gradually increased along the Thio River

449   from 11 % in upper parts to reach 52-58 % in the estuary. On the contrary, non-mining contributions

450   gradually decreased from 56 % in uppermost parts to reach 35-36 % in the estuary (Figure 8-b, Table

451   5).

452   In summary, the FDVS-PLSR models provided opposite results to those of the conventional

453   sediment fingerprinting approach (i.e. 'geochemistry' and 'colour + geochemistry' models). According

454   to the FDVS-PLSR models, non-mining tributaries contributed the majority of the sediment supply for

455   the 2015 (58 %, SD 18 %) and 2017 (51 %, SD 11 %) flood events. On the contrary, the 'geochemistry'

456   and 'colour + geochemistry' models demonstrated that mining tributary contributions dominated

457   sediment supply for the 2015 (i.e. respectively 65 % (SD 27%) and 68 % (SD 28 %)) and 2017 flood

458   events (i.e. respectively 83% (SD 8%) and 88 % (SD 8%)).

459
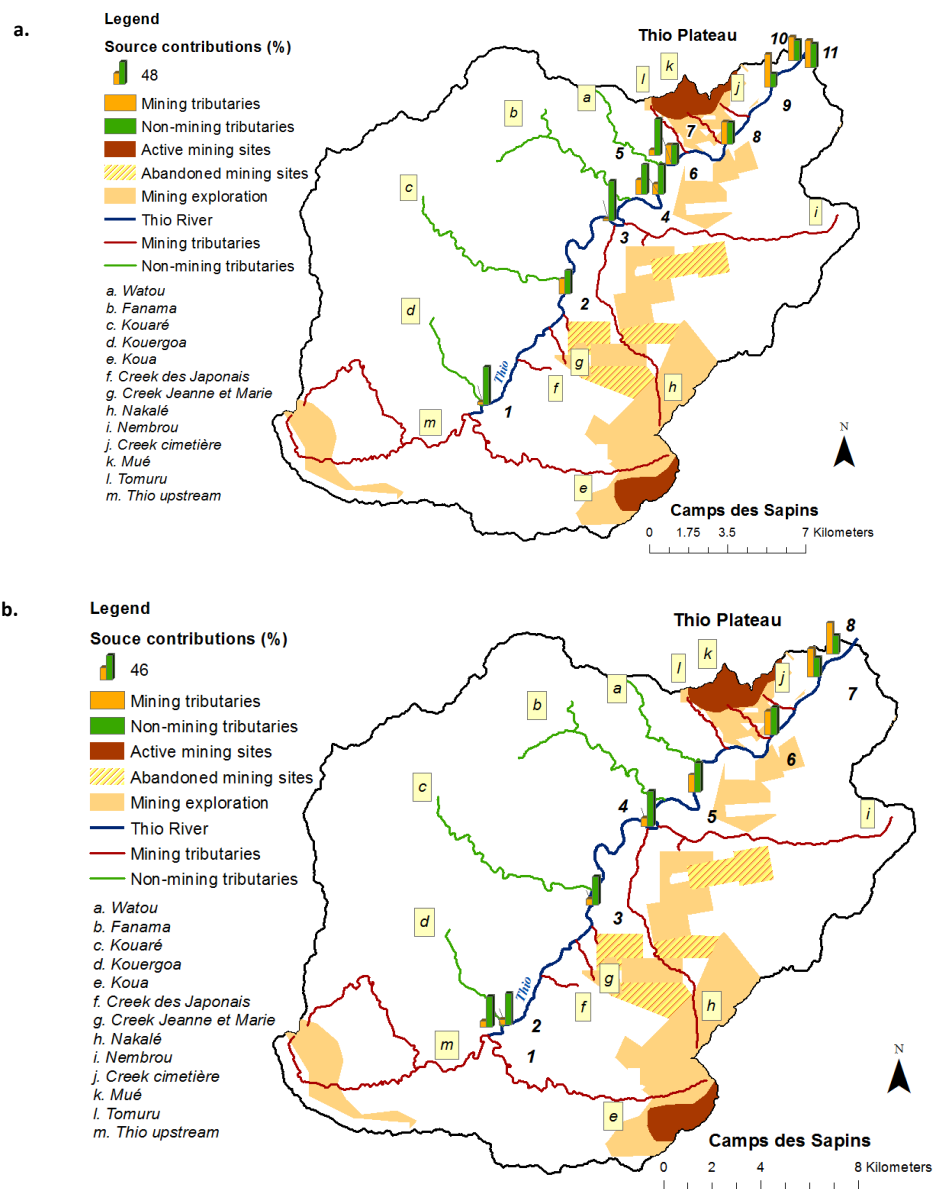
Figure 8 Relative contributions of mining and non-mining tributaries to the sediment collected in the Thio River during the 2015 (a) and 2017 (b) flood events using the FDVS-PLSR models

Table 4 Source contributions calculated by FDVS-PLSR, 'geochemistry', 'colour + geochemistry' approaches for sediment deposited during the flood of February 25,2015

Sampling point	Mining tributary contributions (%)			Non-mining tributary contributions (%)			Sum of source contributions (%)		
	FDS- PLSR	Geochemistry	Colour + Geochemistry	FDS- PLSR	Geochemistry	Colour + geochemistry	FDS- PLSR	Geochemistry	Colour + geochemistry
1	6	96	99	80	4	1	86	100	100
2	33	95	96	51	5	4	84	100	100
3	4	17	17	85	83	83	90	100	100
4	32	65	65	64	35	35	96	100	100
5	22	41	59	63	59	41	85	100	100
6	42	77	74	41	23	26	83	100	100
7	12	29	34	79	71	66	91	100	100
8	47	85	83	46	15	17	93	100	100
9	70	88	89	28	12	11	98	100	100
10	51	64	70	44	36	30	94	100	100
11	59	60	58	52	40	42	111	100	100
M (%)	34	65	68	58	35	32	92	100	100
SD (%)	22	27	25	18	27	25	8	-	-
Minimum (%)	4	17	17	28	4	1	84	-	-
Maximum (%)	70	96	99	85	83	83	111	-	-

Table 5 Source contributions calculated by FDVS-PLSR, 'geochemistry', 'colour + geochemistry' approaches for sediment deposited during the flood of April 10,2017

Sampling point	Mining tributary contributions (%)			Non-mining tributary contributions (%)			Sum of source contributions (%)		
	FDS- PLSR	Geochemistry	Colour + Geochemistry	FDS- PLSR	Geochemistry	Colour + geochemistry	FDS- PLSR	Geochemistry	Colour + geochemistry
1	11	90	100	56	10	0	66	100	100
2	9	94	98	58	6	2	68	100	100
3	11	89	92	52	11	8	63	100	100
4	16	69	74	66	31	26	82	100	100
5	32	82	89	54	18	11	86	100	100
6	44	81	84	51	19	16	95	100	100
7	52	77	83	36	23	17	88	100	100
8	58	83	85	35	17	15	92	100	100
M (%)	29	83	88	51	17	12	80	100	100
SD (%)	20	8	8	11	8	8	13	-	-
Minimum (%)	9	69	74	35	6	0	63	-	-
Maximum (%)	58	94	100	66	31	26	95	-	-

466 **1.6. Complementary tests: representativeness of artificial mixture samples used for the**

467 **FDVS-PLSR models compared to source samples**

468 Given the opposite results obtained in terms of source contributions between FDVS-PLSR

469 models on the one hand and 'geochemistry' and 'colour + geochemistry' models on the other hand,

470 complementary analyses were carried out on individual source samples (i.e. not the composite

471 samples used to create the artificial mixtures) to estimate their composition in terms of source

472 contributions with FDVS-PLSR models. As done in Legout et al. (2013) to assess uncertainties in the

473 fingerprinting approach due to source heterogeneity, they were considered as river sediment

474 samples. A mean sum of the predicted source proportions of 94 % (SD 17 %, range: 49-131 %) was

475 calculated from the source sample data set. The compositions of mining and non-mining tributary

476 samples in Figures 9 and 10 show that artificial mixture samples built from a mix between the

477 composite mining source sample and the composite non-mining source sample did not cover entirely

478 the range of values found in all the sources samples, which may explain why some source samples

479 showed mining and non-mining tributary composition lower than 0 and/or higher than 100 %.
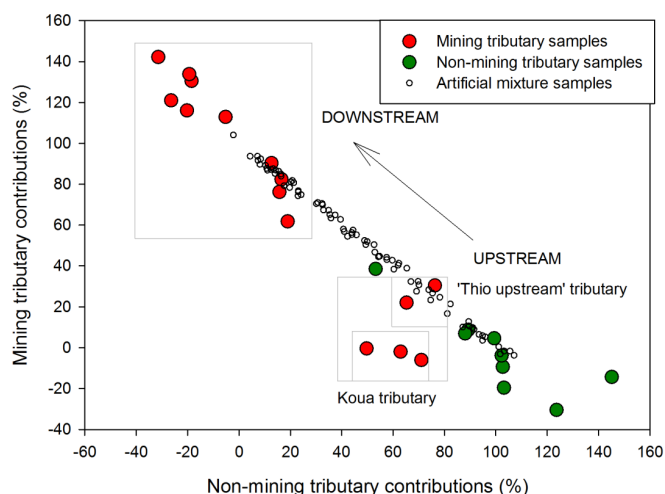
480

481 **Figure 9** Relative compositions of mining and non-mining sources estimated by the FDVS-PLSR models

482 applied to the individual source sediment samples

483   Moreover, two sub-groups of mining tributary samples can be distinguished, the first one

484   corresponding to samples collected on the mining tributaries located in the uppermost part of the

485   catchment and the second to samples collected on the mining tributaries located further

486   downstream. The FDVS-PLSR differentiated rather well the second group since the mining tributary

487   composition is dominant in these samples. On the contrary, the first group referred to as 'Upstream'

488   merged with the non-mining tributary samples (Figure 9). Indeed, Figure 10 shows the mining

489   tributaries located in the upper part of the catchment were defined as 'non-mining tributaries' by the

490   FDVS-PLSR model.
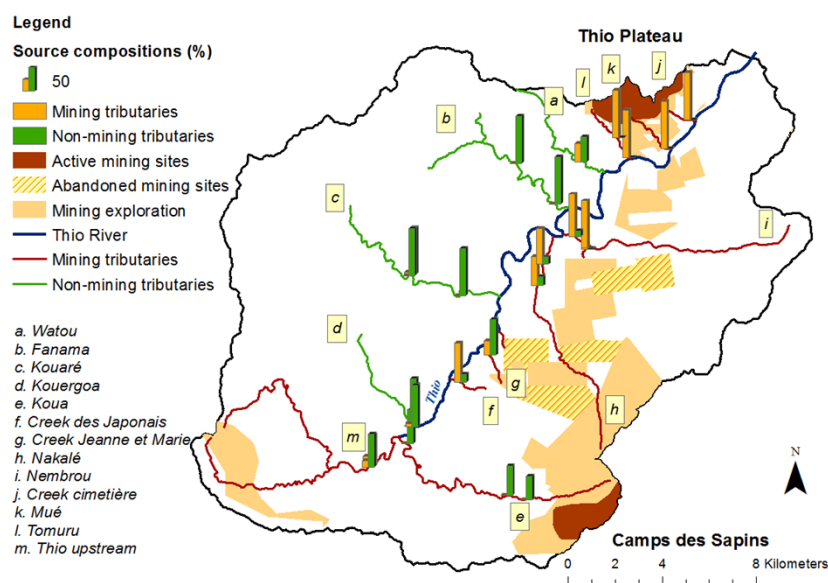
491   **Figure 10** Relative compositions of mining and non-mining sources estimated by the FDVS-PLSR models applied
492   to the individual sediment sources in the Thio River catchment

493   The low K contents found in these samples confirmed, however, that they were mainly

494   supplied by mining sources (Figure 11). Nevertheless, a colour difference could be observed visually

495   and through variations of the a* parameter: the a* values increased from upper parts to lower,

496   which results in an increasingly red coloration of mining tributary samples in downstream direction.

497   Figure 11 shows also that the a* values found in samples collected in the upper catchment part

498   overlapped with those of non-mining tributary samples. Among the 'upstream' mining tributary

499   samples, only three samples collected on the Koua tributary (i.e. draining Camps des Sapins mine)

500   showed values that were not comprised in the ranges covered by the artificial mixture samples

501   (Figure 9).
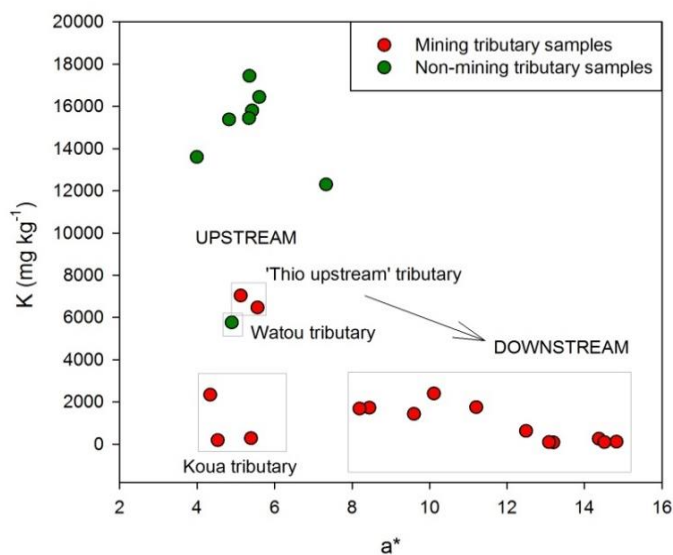
502   **Figure 11** Diagram of K contents as a function of a* parameter values within sediment sources and artificial

503   mixture samples

504   Discussion

505   **1.7.Advantages and limits of models**

506   1.7.1.'Colour' model

507   One of the objectives of this study was to test the contribution of spectrocolorimetry for

508   improving the source discrimination. Indeed, visual observations indicated that mining tributary

509   samples were red-orange whereas non-mining tributary samples were rather grey. However, the

510   results showed that the colour parameters, when used individually, did not provide sufficient

511   discrimination between sources (Table 2) to meet this objective. Indeed, some mining tributary

512   samples showed colour parameter values similar to those found in non-mining tributary samples

513   (e.g. v' at Table 3, or a* shown at Figure 11). This overlap of value ranges could explain in particular

514   the inability of the 'colour' model to provide satisfactory source discrimination. Nevertheless, results

515   obtained with colour parameter analyses coupled to visual observations highlighted the occurrence

516   of two groups of mining tributary samples (i.e. 'Upstream' and 'Downstream'). The coloration

517   differences (i.e. orange/ 'Upstream' and 'red/Downstream') observed between these two groups

518   could be due to the the fact that on the one hand, the reddish colour does not provide a highly

519   conservative signature as it may be altered by the oxydo-reduction of iron minerals during the

520   periods of submersion of sediments under water. On the other hand, the presence of different types

521   of nickel ores could explain these coloration differences. Indeed, nickel ore formation depends partly

522   on the morphological context, for instance on whether nickel ores are located in a basin, on a plateau

523   or a slope. This morphological context influences the weathering level of peridotites (i.e. laterite

524   profile: red laterites at the top >> yellow laterites >> saprolites >> peridotites at the bottom). In the

525   Thio River catchment, nickel ores from the Thio Plateau mine are 'plateau nickel ores' whereas those

526   from the Camps des Sapins mine are 'slope nickel ores' (Mardhel et al., 2018). No information is

527   provided in the literature on the types of nickel ores that were mined in abandoned mining sites. The

528   red coloration of the 'Downstream' mining tributary samples could then be associated with more

529   altered laterite profiles with a thicker layer of red laterites compared to the 'Upstream' mining

530   tributary samples, which could be associated with a laterite profile with a thinner layer of red

531   laterites.

532   1.7.2.'Geochemistry' model

533   The 'geochemistry' model based on K provided significant discrimination between sources

534   (Table 2), regardless of the types of nickel ores that may be found in the Thio River catchment. K is a

535   lithological tracer discriminating sediments originating from the erosion of the two dominant

536   lithologies (i.e. peridotite massifs vs. volcano-sedimentary formations) in the Thio River catchment.

537   As anthropogenic erosion (i.e. due to mining activities) dominates on the peridotite massifs (Garcin

538   et al., 2017), K therefore provides an optimal discrimination between mining and non-mining

539   tributary contributions.

540   This parameter classified the source samples rather well (i.e. 95.3 % of correct classification,

541   Table 3). Indeed, the 16 mining source samples were all correctly classified (100%) and only one non-

542   mining source sample was not correctly classified (87.5 %); it corresponds to the Watou tributary

543   sample (Figure 11). This sample showed a K content similar to that found in mining tributary samples.

544   The Watou tributary is particular because it drains both volcano-sedimentary formations and

545   peridotite massifs that were not exploited for mining, which justifies that it was considered as a non-

546   mining tributary. The K content measured in this sample could be representative of that found in

547   sediment sources characterized by a mix between the two dominant lithologies. Again, when

548   observing Figure 11, two mining tributary samples (i.e. 'Thio upstream') showed similar K contents to

549   that found in the Watou tributary sample. The 'Thio upstream' tributary also drains both areas

550   associated with volcano-sedimentary formations and exploited peridotite massifs (i.e. mining

551   prospection), which justifies that it was considered as a mining tributary.

552   The analysis of colour parameters coupled with that of geochemical elements indicated that

553   these samples collected on the 'Thio upstream' tributary showed a less red coloration not because

554   they are associated with a different type of ore, as could be the case for the samples collected on

555   Koua tributary draining Camps des Sapins mine (Figure 11), but because they are characterized by a

556   mix of both lithologies. As a result, the 'geochemistry' model showed a certain limitation to classify

557   source samples characterized by a mix of both lithologies. The performance of the 'geochemistry'

558   model described in Table 2 remains, however, excellent. The application of this model on artificial

559   mixture samples provided very satisfactory results (Figure 3-a) with a good correlation between the

560   predicted and the actual source proportions (r^2= 0.99). An overestimation of mining tributary

561   contributions is, however, to be taken into account. It was evaluated to a maximum at 15.5 %. This

562 overestimation is greater when the mining contributions estimated by the model tend towards 0 %

563 (maximum: 15.5 %, Figure 3-a).

564 1.7.3. 'Colour + geochemistry' model

565 The 'colour + geochemistry' (i.e. K, Ca, Ti, b*, C*) model provided the best discrimination

566 between sources (Table 3). The inclusion of colour parameters in the 'colour + geochemistry'

567 approach allowed for the discrimination of source samples (i.e. 100 % of correctly classified source

568 samples) that a 'geochemistry' approach alone could not achieve. Results of the tests carried out on

569 the artificial mixture samples also showed an excellent correlation between the predicted and the

570 actual source proportions (i.e. $r^2 = 0.98$). A slight overestimation of the mining tributary contributions

571 (7 %) was observed with this approach, which remains rather reasonable (Figure 3-b). In this model, K

572 is the lithological tracer which has the higher discriminant powerful (Table 2), which may explain the

573 similarity of results obtained with the 'colour + geochemistry' and the 'geochemistry' models.

574 Indeed, mining tributaries contributed an average of 65 % (SD 27 %) for 'colour + geochemistry'

575 model and 68 % (SD 25 %) for 'geochemistry' model (Table 4). For the 2017 flood event, mining

576 source contributions largely dominated the sediment production with a mean contribution of 83 %

577 (SD 8 %) for the 'geochemistry' model and 88 % (SD 8 %) for the 'colour + geochemistry' model.

578 1.7.4. FDVS-PLSR models

579 The FDVS-PLSR models built from artificial mixture samples showed excellent theoretical

580 predictive performances (e.g. r^2, RMSEC, RMSEC, Figure 5). However, the application of these models

581 on river sediment samples provided questionable results. Indeed, the artificial mixture samples did

582 not cover entirely the ranges of values found in all sources samples, thus resulting in an

583 overestimation (i.e. superior to 100 %) and an underestimation (i.e. inferior to 0 %) of source

584 composition (Figure 9) in several source samples. Similarly to what was previously observed, three

585 sub-groups of mining tributary samples can be distinguished, one of which (i.e. 'Thio Upstream') is

586 partially merged with the non-mining tributary samples (Figure 9). When modelling the source

587   contributions with the FDVS-PLSR models, a bias was created because the contributions of this

588   mining tributary may be mainly considered as the contributions of non-mining tributaries. As a result,

589   an overestimation of non-mining tributary contributions may be found in the entire Thio River

590   catchment and particularly in the upper part of the study area. Third, the properties measured in the

591   Koua tributary (i.e. draining Camps des Sapins Mine) samples were not comprised in the ranges of

592   values covered by the artificial mixture samples (Figure 9).

593   Given the particular colour signature of this tributary (Figure 11), its contributions are

594   therefore not taken into account at all by the FDVS-PLSR models. Indeed, the sums of the source

595   contributions by FDVS-PLSR models are lower than the expected 100% particularly in the uppermost

596   part of the catchment (Tables 4 and 5), which may indicate that a source is not accounted for.

597   Artificial mixtures were constructed from a homogenized spectral signature of all mining source

598   samples. However, two distinct spectral signatures were observed between the upstream and

599   downstream mining source samples. Homogenizing the spectral signature of the mining samples led

600   to a loss of information in terms of spectral signature, in particular that of the mining samples

601   located upstream. As a result, a 3-source FDVS-PLSR models (i.e. non-mining, upstream and

602   downstream mining sources) would have been more appropriate than 2-source FDVS-PLSR models in

603   this context.

604   **1.8.Spatial and temporal variations of sediment source contributions**

605   Among the four models tested in this study, the 'colour + geochemistry' model is the most

606   appropriate to estimate mining and non-mining tributary contributions in the Thio River catchment.

607   According to the results of this model, mining tributaries provided the main sediment supply to the

608   river system with a mean contribution of 68 % (SD 25 %) for the 2015 flood event and 88 % (SD 8 %)

609   for the 2017 flood event (Tables 4 and 5). The variability of mining tributary contributions between

610   these two flood events with a return period of 10 years (3500 $m^3 s^{-1}$) could be explained in particular

611   by the variability of rainfall distribution (Sellier et al., 2019). Indeed, during the 2015 flood event, the

612   Kouaré River sub-catchment received twice the rainfall than observed in the rest of the Thio River

613   catchment, which may explain a higher contribution of non-mining tributaries for this event than for

614   the 2017 flood event where rainfall was more intense on the eastern part of the catchment in the

615   vicinity of the mines currently in operation (Thio Plateau, Camps des Sapins).

616   Although the FDVS-PLSR models were unable to properly estimate the source contributions,

617   they provided qualitative indications about the proportion of sediment contribution between

618   'Upstream' and 'Downstream' mining tributaries at the level of the estuary. Indeed, only

619   'downstream' mining tributaries were finally identified by the FDVS-PLSR models as mining sources.

620   Mining contributions gradually increased in downstream direction. The predicted proportion sums of

621   river sediment samples also tend to reach the expected 100%, which could result in a better

622   predictability of the models. As a result, these models indicated that sediment contribution from

623   downstream reaches dominated that of upstream reaches at the level of the estuary for both events.

624   Moreover, the analysis of colour parameters coupled to that of geochemical elements

625   highlighted the occurrence of three sub-groups of mining tributary samples, (1) 'Downstream'

626   samples characterized by high a* values and low K contents, (2) 'Koua tributary' samples located in

627   the upstream characterized by low a* values and low K contents and (3) 'Thio upstream' samples

628   corresponding to a mix of both dominant lithologies (i.e. peridotite massifs and volcano-sedimentary

629   formations) characterized by low a* values and higher K contents (i.e. 4 times higher than for the

630   two previous sub-groups) (Figure 11). Owing to the low K contents found in Thio River sediment

631   samples collected in the uppermost part (i.e. ~ 2200 mg kg^{-1} in 2015 and ~ 2600 mg kg^{-1} in 2017),

632   which were similar to those measured in samples of sub-group (2, ~2400 mg kg^{-1}), it would appear

633   that the Koua tributary draining Camps des Sapins mine dominated the sediment supply in the

634   upstream for both events.

635   Conclusions

636   The current study showed that the contributions of mining sources dominated the sediment

637   inputs with mean contributions of 68 % (SD 25 %) for the 2015 flood event and 88 % (SD 8 %) for the

638   2017 flood event (results of 'colour + geochemistry' model). Although the spatial variability of rainfall

639   may impact local sediment source contributions, a trend in terms of sediment source contributions is

640   observed along the Thio River for both flood events. In the uppermost part of the catchment, mining

641   source contributions dominated (99% in 2015, 100% in 2017) with a dominant contribution from the

642   Koua tributary draining the Camps des Sapins mine. The first non-mining tributary encountered in

643   downstream direction (i.e. the Kouergoa tributary) contributed little to sediment supply; it is rather

644   the next non-mining tributaries (i.e. the Kouaré tributary) which provided most of the sediment

645   inputs (83 % in 2015, 26 % in 2017). Nevertheless, these contributions were compensated in

646   downstream direction by those from mining sources generated by tributaries draining Thio Plateau

647   mine. Finally, at the estuary, mining sources dominated (58-70% in 2015, 83-85 % in 2017). These

648   results therefore suggest that catchment management should focus on mining tributaries draining

649   active mining sites (i.e. Camps des Sapins and the Thio Plateau).

650   One of the objectives of this study was to evaluate the performance of sediment tracing

651   methods based on spectroscopy measurements (i.e. colour parameters and FDVS). The results

652   showed that these individual fingerprinting approaches did not provide sufficient discrimination

653   between sources to be used for the modelling of sediment source contributions. Nevertheless, the

654   inclusion of colour properties in addition to geochemical parameters turned out to be the optimal

655   combination of tracers providing the highest discrimination between sediment sources. This 'colour +

656   geochemistry' model is, however largely based on the discriminatory power provided by K, which

657   means that the 'geochemistry' approach is also relevant to quantify sediment sources. Both

658   approaches have, moreover, been experimentally validated. As a result, the use of these approaches

659   could be extended to other mining catchments of New Caledonia but also to other similar nickel

660   mining catchments (i.e. Ni oxidized ores based on peridotite massifs) around the world (e.g.

661   Australia, Brazil, Dominican Republic, Cuba).

662   **Data availability**

663   The database has been registered on the PANGEAE website and is currently undergoing the editorial

664   process: https://issues.pangaea.de/browse/PDI-25229.

665   Author contribution

666   Oldrich Navratil, Michel Allenbach and Olivier Evrard designed research. Virginie Sellier, Oldrich

667   Navratil, Olivier Evrard and Irène Lefèvre carried out fielwork sampling. Virginie Sellier conducted the

668   analyses. All co-authors contributed to data analysis and interpretation. John Patrick Laceby

669   contributed to modelling. All co-authors contributed to the writing and approved the final version of

670   the manuscript.

671   Competing interests

672   The authors declare that they have no conflict interest.

673   **Acknowledgements**

674   This work was funded by the National Technical Research Center (CNRT) "Nickel and Its

675   Environment", Noumea, New Caledonia » (n°10PS2013-CNRT.UNC/IMMILA). The PhD project of

676   Virginie Sellier is also financed by the French Atomic Energy Commission (CEA, Commissariat à

677   l'Energie Atomique et aux Energies Alternatives). The authors are grateful to Jean-Guy M'Boueri,

678   Pierre Chanel, Jean-Jean, Lorenza M'Boueri, Nicolle Mathys for their invaluable support to identify

679   and have access to the field sampling sites.

680

681   References

682   Abel, A., Michael, A., Zartl, A., and Werner, F.: Impact of erosion-transported overburden dump
683   materials on water quality in Lake Cospuden evolved from a former open cast lignite mine south of
684   Leipzig, Germany, Environmental Geology, 39, 683-688, 2000.
685   Baudrimont, M., Dominique, Y., Feurtet-Mazel, A., Gonzalez, P., Gourvès, P.-Y., Gunkel-Grillon, P.,
686   Laporte-Magoni, C., Lefrançois, E., Letourneur, Y., Marquié, J., Maury-Brachet, R., Monna, F.,
687   Pasquet, C., Rivière, E., and Roth, E.: - Rapport scientifique final. Programme « Dispersion des métaux
688   de la mine au lagon. ». CNRT « Nickel & son environnement ». 192 pages, 2019.
689   Bird, E. C. F., Dubois, J. P., and Iltis, J. A.: The impacts of opencast mining on the rivers and coasts of
690   New Caledonia. Tokyo, Japan, United Nations University, 1984.
691   Blake, W. H., Wallbrink, P. J., Wilkinson, S. N., Humphreys, G. S., Doerr, S. H., Shakesby, R. A., and
692   Tomkins, K. M.: Deriving hillslope sediment budgets in wildfire-affected forests using fallout
693   radionuclide tracers, Geomorphology, 104, 105-116, 10.1016/j.geomorph.2008.08.004, 2009.
694   Bradley, S., and Lewin, J.: Transport of heavy metals on suspended sediments under high flow
695   conditions in a mineralised region of Wales, Environmental Pollution Series B, Chemical and Physical,
696   4, 257-267, 1982.
697   Brosinsky, A., Foerster, S., Segl, K., and Kaufmann, H.: Spectral fingerprinting: sediment source
698   discrimination and contribution modelling of artificial mixtures based on VNIR-SWIR spectral
699   properties, Journal of soils and sediments, 14, 1949-1964, 2014.
700   Collins, A., Walling, D., and Leeks, G.: Use of the geochemical record preserved in floodplain deposits
701   to reconstruct recent changes in river basin sediment sources, Geomorphology, 19, 151-167, 1997.
702   Collins, A. L., Walling, D. E., and Leeks, G. J. L.: Composite fingerprinting of the spatial source of fluvial
703   suspended sediment : a case study of the Exe and Severn river basins, United Kingdom,
704   Géomorphologie, 2, 41-53, 10.3406/morfo.1996.877, 1996.
705   Danloux, J., and Laganier, R.: Classification et quantification des phénomènes d'érosion, de transport
706   et de sédimentation sur les bassins touchés par l'exploitation minière en Nouvelle Calédonie, 1991.
707   Daszykowski, M., Walczak, B., and Massart, D.: Representative subset selection, Analytica chimica
708   acta, 468, 91-103, 2002.
709   Debret, M., Sebag, D., Desmet, M., Balsam, W., Copard, Y., Mourier, B., Susperrigui, A.-S., Arnaud, F.,
710   Bentaleb, I., and Chapron, E.: Spectrocolorimetric interpretation of sedimentary dynamics: the new
711   "Q7/4 diagram", Earth-Science Reviews, 109, 1-19, 2011.
712   Dumas, P., Printemps, J., Mangeas, M., and Luneau, G.: Developing erosion models for integrated
713   coastal zone management: A case study of The New Caledonia west coast, Marine Pollution Bulletin,
714   61, 519-529, 2010.
715   Evrard, O., Laceby, J. P., Huon, S., Lefèvre, I., Sengtaheuanghoung, O., and Ribolzi, O.: Combining
716   multiple fallout radionuclides (137Cs, 7Be, 210Pbxs) to investigate temporal sediment source
717   dynamics in tropical, ephemeral riverine systems, J Soils Sediments, 16, 1130-1144, 10.1007/s11368-
718   015-1316-y, 2015.
719   Evrard, O., Durand, R., Foucher, A., Tiecher, T., Sellier, V., Onda, Y., Lefèvre, I., Cerdan, O., and
720   Laceby, J. P.: Using spectrocolourimetry to trace sediment source dynamics in coastal catchments
721   draining the main Fukushima radioactive pollution plume (2011–2017), Journal of Soils and
722   Sediments, 1-12, 2019.
723   Evrard, O., Chaboche, P.-A., Ramon, R., Foucher, A., and Laceby, J. P.: A global review of sediment
724   source fingerprinting research incorporating fallout radiocesium (137Cs), Geomorphology, 107103,
725   2020.
726   Garcin, M.: Exploitation des granulats en lit vif des cours d'eau de la Grande-Terre, Nouvelle-
727   Calédonie. BRGM/RP-58531-FR. 114 p., 90 fig., 3 tabl., Bureau des Recherches Géologiques et
728   Minières 2010.

729 Garcin, M., Gastaldi, Y., and Lesimple, S.: Quantification et évolution temporelle des apports miniers
730 dans les rivières calédoniennes. BRGM/RP-66840-FR, 44 p., 23 fig., 5, Bureau des Recherches
731 Géologiques et Minières

732 2017.
733 Hedouin, L., Pringault, O., Metian, M., Bustamante, P., and Warnau, M.: Nickel bioaccumulation in
734 bivalves from the New Caledonia lagoon: Seawater and food exposure, Chemosphere, 66, 1449-1457,
735 2007.
736 Highley, D., Chapman, G. R., and Bonel, K.: The economic importance of minerals to the UK, British
737 Geological Survey, 2004.
738 Iltis, J.: La mine, élement de la controverse écologique dans le Pacifique Sud, L'Espace géographique,
739 193-205, 1992.
740 Juillot, F.: – Rapport scientifique final. Programme « Dynamique des métaux de la mine au lagon ».
741 CNRT « Nickel & son environnement ». 202 pages., 2019.
742 Klages, M., and Hsieh, Y.: Suspended Solids Carried by the Gallatin River of Southwestern Montana:
743 II. Using Mineralogy for Inferring Sources 1, Journal of Environmental Quality, 4, 68-73, 1975.
744 Laceby, J. P., and Olley, J.: An examination of geochemical modelling approaches to tracing sediment
745 sources incorporating distribution mixing and elemental correlations, Hydrol. Process., 29, 1669-
746 1685, 10.1002/hyp.10287, 2015.
747 Laceby, J. P., Evrard, O., Smith, H. G., Blake, W. H., Olley, J. M., Minella, J. P. G., and Owens, P. N.: The
748 challenges and opportunities of addressing particle size effects in sediment source fingerprinting: A
749 review, Earth-Sci. Rev., 169, 85-103, 10.1016/j.earscirev.2017.04.009, 2017.
750 Legout, C., Poulenard, J., Nemery, J., Navratil, O., Grangeon, T., Evrard, O., and Esteves, M.:
751 Quantifying suspended sediment sources during runoff events in headwater catchments using
752 spectrocolorimetry, J Soils Sediments, 13, 1478-1492, 10.1007/s11368-013-0728-9, 2013.
753 Mardhel, V., Iseppi, M., Regninger, P. A., and Sevin, B.: Connaissance de l'ophiolite, géophysique
754 aéroportée et étude de la structure. Rapport scientifique final. Programme «OPHIOSTRUCT». CNRT
755 «Nickel & son environnement», 2018.
756 Martínez-Carreras, N., Udelhoven, T., Krein, A., Gallart, F., Iffly, J. F., Ziebel, J., Hoffmann, L., Pfister,
757 L., and Walling, D. E.: The use of sediment colour measured by diffuse reflectance spectrometry to
758 determine sediment sources: application to the Attert River catchment (Luxembourg), J Hydrol, 382,
759 49-63, 2010.
760 Pascal, N.: Ecosystèmes coralliens de Nouvelle-Calédonie. Valeur économique des services
761 écosystémiques. Partie I: Valeur financière. IFRECOR., 2010.
762 Poulenard, J., Perrette, Y., Fanget, B., Quetin, P., Trevisan, D., and Dorioz, J.-M.: Infrared
763 spectroscopy tracing of sediment sources in a small rural watershed (French Alps), Science of the
764 Total Environment, 407, 2808-2819, 2009.
765 Poulenard, J., Legout, C., Nemery, J., Bramorski, J., Navratil, O., Douchin, A., Fanget, B., Perrette, Y.,
766 Evrard, O., and Esteves, M.: Tracing sediment sources during floods using Diffuse Reflectance
767 Infrared Fourier Transform Spectrometry (DRIFTS): A case study in a highly erosive mountainous
768 catchment (Southern French Alps), Journal of Hydrology, 414, 452-462, 2012.
769 Prior, T., Daly, J., Mason, L., and Giurco, D.: Resourcing the future: Using foresight in resource
770 governance, Geoforum, 44, 316-328, 2013.
771 Rossel, R. V., Walvoort, D., McBratney, A., Janik, L. J., and Skjemstad, J.: Visible, near infrared, mid
772 infrared or combined diffuse reflectance spectroscopy for simultaneous assessment of various soil
773 properties, Geoderma, 131, 59-75, 2006.
774 Sellier, V., Navratil, O., Laceby, J. P., Allenbach, M., Lefèvre, I., and Evrard, O.: Investigating the use of
775 fallout and geogenic radionuclides as potential tracing properties to quantify the sources of
776 suspended sediment in a mining catchment in New Caledonia, South Pacific, Journal of Soils and
777 Sediments, 1-17, 2019.

778 Shellberg, J., Brooks, A., and Spencer, J.: Land-use change from indigenous management to cattle
779 grazing initiates the gullying of alluvial soils in northern Australia, 19th World Congress of Soil
780 Science: Soil Solutions for a Changing World, 2010, 1-6,
781 Sherriff, S. C., Franks, S. W., Rowan, J. S., Fenton, O., and Ó'hUallacháin, D.: Uncertainty-based
782 assessment of tracer selection, tracer non-conservativeness and multiple solutions in sediment
783 fingerprinting using synthetic and field data, J Soils Sediments, 15, 2101-2116, 10.1007/s11368-015-
784 1123-5, 2015.
785 Smith, H. G., Sheridan, G. J., Lane, P. N. J., Noske, P. J., and Heijnis, H.: Changes to sediment sources
786 following wildfire in a forested upland catchment, southeastern Australia, Hydrol. Process., 25, 2878-
787 2889, 10.1002/hyp.8050, 2011.
788 Surell, A.: Étude sur les torrents des Hautes-Alpes, Carilian-Goeury, 1841.
789 Tiecher, T., Caner, L., Minella, J. P., and dos Santos, D. R.: Combining visible-based-color parameters
790 and geochemical tracers to improve sediment source discrimination and apportionment, Sci Total
791 Environ, 527-528, 135-149, 10.1016/j.scitotenv.2015.04.103, 2015.
792 Uber, M., Legout, C., Nord, G., Crouzet, C., Demory, F., and Poulenard, J.: Comparing alternative
793 tracing measurements and mixing models to fingerprint suspended sediment sources in a mesoscale
794 Mediterranean catchment, Journal of Soils and Sediments, 1-19, 2019.
795 Vaithiyanathan, P., Ramanathan, A., and Subramanian, V.: Transport and distribution of heavy metals
796 in Cauvery River, Water, Air, and Soil Pollution, 71, 13-28, 1993.
797 Walden, J., Slattery, M. C., and Burt, T. P.: Use of mineral magnetic measurements to fingerprint
798 suspended sediment sources: approaches and techniques for data analysis, Journal of Hydrology,
799 202, 353-372, 1997.
800 Wallbrink, P., Murray, A., Olley, J., and Olive, L.: Determining sources and transit times of suspended
801 sediment in the Murrumbidgee River, New South Wales, Australia, using fallout 137Cs and 210Pb,
802 Water Resour Res, 34, 879-887, 1998.
803 Wallbrink, P. J.: Quantifying the erosion processes and land-uses which dominate fine sediment
804 supply to Moreton Bay, Southeast Queensland, Australia, Journal of environmental radioactivity, 76,
805 67-80, 2004.
806 Walling, D., Peart, M., Oldfield, F., and Thompson, R.: Suspended sediment sources identified by
807 magnetic measurements, Nature, 281, 110, 1979.
808 Yellishetty, M., Mudd, G. M., and Shukla, R.: Prediction of soil erosion from waste dumps of opencast
809 mines and evaluation of their impacts on the environment, International Journal of Mining,
810 Reclamation and Environment, 27, 88-102, 2013.

811